Egypt. J. Chem. **Vol. 65,** No. SI:13B pp. 203 - 211 (2022)

Egyptian Journal of Chemistry

http://ejchem.journals.ekb.eg/

Preparation and investigation of the corrosion inhibitor behavior of deposited nanocomposite on carbon steel in the oil industry

1 Naeem A. Basher , [2]Ali Abdulkhabeer Ali

[1]Science of college- Chemistry department/ University of Thi-Qar/ Iraq

[2]Science of college- Chemistry department/ University of Thi-Qar/ Iraq

[2] Marshes research center-University of Thi-Qar/ Iraq

Abstract

In this research, Al2O3.B2O3 nanoparticles were synthesized by co-precipitation method and modified by coating with 2,2'-((1E,1'E)-((1,3,4-thiadiazole-2,5-diyl)bis(hydrazin-2-yl-1-ylidene))bis(methaneylylidene))bis(4-(octadecyloxy)phenol) [BITT]. For the first time, the nano-aluminum borates compound was obtained by precipitation at room temperature using aluminum oxide nanoparticles as a precursor. In this study, a new nanocomposite was prepared from inorganic nanoparticles of aluminum borates (Al2O3.B2O3) with the heterocyclic compound [BITT] and investigated for the efficiency of nanocomposit inhibition on carbon alloy by using an electrochemical method. The crystal structure of the Al2O3.B2O3-[BITT] nanocomposite was investigated by X-ray diffraction, Fourier transform infrared spectroscopy (FT-IR) and 1H-NMR spectra. The analysis (FESEM) , (AFM) and (TEM) were used to determine particle size and the surface morphology. The efficiency of the prepared nanocomposite was evaluated using the potentiodynamic polarization measurements (Tafel plot) method on carbon steel (C45) specimens. It is a type identical to some of the metal types used in the Halfaya complex in Maysan governorate in the oil fields of southern Iraq. Through the practical results obtained , Noted that the results of the inhibition efficiency (IE) of the prepared nanocomposite Al2O3.B2O3-[BITT] was high values. The highest inhibition efficiency was at the concentration (100) ppm where it reached (99.96 %) . Through the results obtained in this study.

Keywords: Nanotechnology, Corrosion inhibitor, Potentiodynamic Polarization Measurements (Tafel plot), Aluminum borates nanocomposite , Al2O3.B2O3-[BITT] .

Introduction

Nano-science is based on the uniqueness of the structural properties, energy, response, dynamics and chemical properties of nanostructures [1]. Nanotechnology is one of the most promising technologies which is expected to lead to major changes and find new materials and products in many fields, particularly medical and industrial [2-4].due to their remarkable characteristics, there has been great interest in nanoparticles in recent years. One of the important applications of nanomaterials is metal corrosion protection. In addition, many research studies have indicated the distinctive properties of nanocomposites and their applications as corrosion inhibitors [5- 7].

Corrosion is defined as the destruction of metals and alloys by the surrounding environment through chemical or electrochemical changes. Corrosion causes many problems of degradation, failure, and serious accidents and dangers in many industrial processes [8, 9]. Corrosion of metals occurs because they react with corrosive elements like chlorine, fluorine, carbon dioxide, oxygen, etc. in their environment. The cost of repair and maintenance, the loss of equipment, damage to equipment, lower efficiencies, and the loss of useful or productive life are economic damages. Moreover, damage to corrosion also has other social impacts, such as fire safety, explosions, toxicity release, health effects, personal injuries, contamination of toxic products, depletion of resources, etc. In particular, it has an effect on human health [10 –13].

Shale oil, a complicated blend of hydrocarbons, is the foundation for global energy savings. The presence of these liquid hydrocarbons can often contribute to minimizing corrosion due to their tendency to form highly adherent coatings on the metal surface. In other circumstances, the presence of contaminants such as

*Corresponding author e-mail: nae.abd_ch@utq.edu.iq.; (Naeem Abdlsada Basher).

Receive Date: 29 January 2022, Revise Date: 30 March 2022, Accept Date: 06 April 2022

DOI: 10.21608/EJCHEM.2022.118829.5350

H_2S and CO_2 naphenic acids may cause corrosion of stainless steel pipes and equipment used in the exploration, production, transport, and petroleum refining activities [14,15]. The presence of chloride ions is the primary cause of pitting corrosion in carbon steel. This is because of their aggressive nature, which is caused by their tiny ionic radius, which allows for higher diffusion between the monolayers created on the metal surface. Corrosion in the petroleum sector may generally be reduced by using inhibitors, which are compounds that reduce the progression of metal corrosion [16,18].

There are widespread efforts in the field of corrosion control, to promote their effective use. For instance, in advanced coating [19-20]. Nanomaterials are key points of availability and economic synthesis. More studies are needed to support nanomaterial use in various corrosion control areas and to authenticate the nanostructured materials' corrosion-oxidation performance [21-23]. One of the main problems in the oil and gas industries, for which a great deal of money is spent each year, is the corrosion of pipelines. Crude oil may include water, salts, hydrogen sulphide, and microbial organisms (NaCl, $CaCl_2$, $MgCl_2$). There are widespread efforts in the field of corrosion control, to promote their effective use. For instance, in advanced coating. Nanomaterials are key points of availability and economic synthesis. More studies are needed to support nanomaterial use in various corrosion control areas and to authenticate the nanostructured materials' corrosion-oxidation performance [24,25] .

H. Hameed et al.,[26], studied the preparation of various derivatives of graphene oxide (GO) by functionalization of GO with each of the following compounds: malicanhydride, 2-amino pyridine, amino ethanol, mercapto ethanol and 2-hydroxy-5-sulfobenzoic acid that contain various heterogeneous atoms (sulfur , nitrogen and oxygen) to get the following compounds: (GOM), (GON_1), (GON_2), (GOS_1) and (GOS_2) respectively and evaluated them as corrosion inhibitors on carbon steel alloys surface at different concentrations (1-6 ppm) and different temperatures (298-328 K) in acidicmedia. The study investigated the effect of temperature on somethermodynamic functions, In this study, it was found that the corrosionrate where the inhibition effect of GO on carbon steel alloy is lesser than its derivatives because its derivatives included atoms of sulfur, nitrogen and oxygen in their composition. This study was involved the optimal concentration for all inhibitors is 6 ppm , where it was found that $GOS_1$and GON_2 inhibitors have higher inhibition efficiency than of other inhibitors which are equal to 95.79% , 96.96 % respectively at optimal concentration and 298 K .

T. Quadri et al., [27]., presented a study that included ZincOxide nanocomposites of Selected Polymers: Synthesis, characterization, and Corrosion Inhibition Studies on Mild Steel in HCl Solution. Polymers such as polyvinylpyrrolidone and polyacrylonitriles are used. The study showed that nanocomposites were tested as mixed inhibitors and inhibited mild steel corrosion better than the respective polymer alone. Nanocomposits were found to adsorb on a mild steel surface more efficiently.

K. Vinothkumar et al, [28], Corrosion inhibition ability of electropolymerised composite film of 2-amino-5-mercapto-1,3,4-thiadiazole/TiO_2 deposited over the copper electrode in neutral medium. Inhibitions of the corrosion capacity of a thiadiazole derivative/TiO_2 film protection demonstrated an inhibition efficiency of 83.42 % .

The aim of this study is to prepare and diagnose the $Al_2O_3.B_2O_3$-[BITT] nanocomposite, in addition, to investigate the surface morphology and characterization of the nanocomposite using various analysis techniques (AFM,XRD, FESEM, TEM, FT-IR and ^1H NMR).Furthermore, the inhibition efficiency of the prepared nanocomposite as a corrosion inhibitor on carbon steel (C45) specimens was tested using the potentiodynamic polarization measurements (Tafel plot) method.

Experimental part :

2.1 Materials and methods :

Many chemicals were used in this work as electrolyte and nanocomposite for achieve the corrosion inhibitors as show in the Table (2.1).

This work includes descriptions of materials and instrumentation used, and procedures for performing corrosion tests on carbon steel (C45) specimens without and with nanocomposite prepared. The chemical composition of carbon steel (C45): these materials are listed in Table (2.2) .

2.2. preparation of corrosion inhibitor [$Al_2O_3.B_2O_3$ - [BITT] nanocomposite

2.2.1. Synthesis of aluminum borate nanoparticles $Al_2O_3.B_2O_3$

The synthesis of $Al_2O_3.B_2O_3$ nanoparticles was performed following the modified method of Vu T Tan et al. [29]. In a typical synthesis, an aqueous solution of aluminum acetate (0.01 mole) was prepared in 100 ml distilled water. Consequently, urea was added to the concentration of (0.02 1 mole) under magnetical stirring. The pH of the solution was adjusted to 4.0, using several drops of concentrated acetic acid. Then the mixture was hydrothermally treated at 80 °C for (12 hr) at a constant temperature. Finally, the precipitated Al $(OH)_3$ was thoroughly washed with distilled water and dried in an oven at 60 °C for several hours. The Al_2O_3 nanoparticles were obtained after the calcination step at 250 °C for (1 hr) in the air. The

fabrication of nano-aluminum borate was done using the Al_2O_3 nanoparticles as the primary precursor with only one-step precipitation method. In a typical synthesis, boric acid H_3BO_3 and Al_2O_3 nanoparticles were mixed in 200 ml of distilled water. The molar ratio between H_3BO_3 and $Al_2O_3$is varied from 1 to 3. The mixture was stirred at a constant room-temperature to obtain the complete precipitation of aluminum borate. The synthesis time was varied from (3 to 6 hr) . After the reaction, the aluminum borate was vacuum filtered and thoroughly washed by distilled water for several times. Finally, the achieved aluminum borate particles were dried in the oven at 50 °C for (15 hr).

Table (2.1): Chemical materials used in this study.

substances	Chemical formula	Purity	Company
Hydrazine hydrate	$NH_2NH_2.H_2O$	99.9%	/Merck Germany
Carbon disulphide	CS_2	99.9%	UK / Romil
Ethanol absolute	CH_3CH_2OH	%99	/Merck Germany
Hydrochloric	HCl	%37	/Merck Germany
Potassium hydroxide	KOH	%98	INDIA/B.D.H
Glacial Acetic Acid	CH_3COOH	%95.5	INDIA/B.D.H
2,5-dihydroxybenzaldehyde	$C_6H_3(OH)_2CHO$	% 98	Merck Germany/
1-Bromooctadecane	$CH_3(CH_2)_{17}$ Br	%97	Merck Germany/
Aluminum acetate	$Al(CH_3COO)_3$	98%	/Merck Germany
Urea	NH_2CONH_2	99%	India/ SDH
Boric acid	H_3BO_3	95.5%	/Merck Germany
Sulfuric acid	H_2SO_4	98%	India/ SDH
Iodine	I_2	99.9%	/Merck Germany

Table (2.2): Metallic materials' chemical composition for carbon steel (C45) specimen

Grade	% C	% Mn	% P	% S	% Si	% Cr	% Ni	%Mo
C45	0.42-0.50	0.50-0.80	<0.045	<0.045	<0.40	<0.40	0.40	<0.10

2.2.2.Preparation compound [BITT]

The hydroxide of potassium (0.3 mole) was dissolved in ethanol (100 ml). After that, (16 ml) of carbon disulfide was added to the solution, and the mixture was heated for (24 -30 hr) (reflex). Follow-up of the reaction by chromatography (TLC). Observe the formation of yellow crystals of the thiadiazole derivative by cooling the product and adding hydrochloric acid (10%) to the reaction mixture. The precipitate was filtered, washed, and recrystallized by used a mixture water and ethanol. 2,5-dithiole-1,3,4-thiadiazole (X_1) product output is around [92%] and the melting point is [163-165] ^oC, as shown in Figure (2.1) [30].

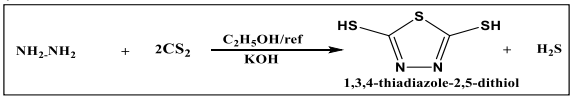

Figure (2.1): synthesis 2,5-dithiole-1,3,4-thiadiazole (X_1)

Mix (0.01 mole) of the compound (X_1) with (0.02 mole) of hydrazine in the reaction flask (Reflex) for a period ranging from (10–12 hr) while continuing the reaction with TLC. The product 2,5-dihydrazinel-1,3,4-thiadiazole (X_2) is filtered, washed, and recrystallized with a mixture of ethanol and water. The product is yellowish-white crystals with a high yield (78%) and the melting point is (195-200 ^oC). The reaction is shown in figure (2.2) [31].

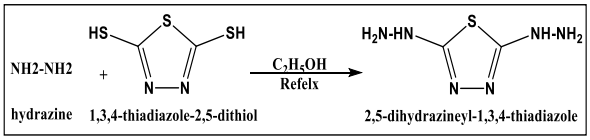

Figure (2.2): synthesis of 2,5-dihydrazinel-1,3,4-thiadiazole (X_2)

dissolved (0.01 mol) 2,5-dihydrazinel-1,3,4-thiadiazole (X2) in 50 mL of absolute ethanol and added (0.02 mol) of 2,5-dihydroxybenzaldehyde in a reaction flask (Reflex) for (3- 4 hr), filtered the precipitate, and the resulting recrystallized by mixing ethanol and water to obtain dark brown crystals of compound (X_3) . The product yield was 80% and the melting point was(200-205) °C. As shown in Figure (2-3) [31].

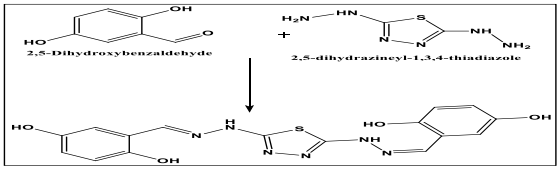

Figure (2.3): synthesis of compound (X_3)

Anhydrous sodium carbonate (0.025 mol) was added to a mixture of (X_3) (0.01 mol) and 1-

bromoctadecane (0.02 mol) dissolved in (15 mL) of (DMF), (refelx) for 4 hours. The reaction mixture was allowed to cool to room temperature before being cooled to (-10°C) and left overnight. The precipitate [BITT] is washed and recrystallized to obtain. As crystals of light brown color and yield (90%) [32] ,as shown in Figure (2.4).

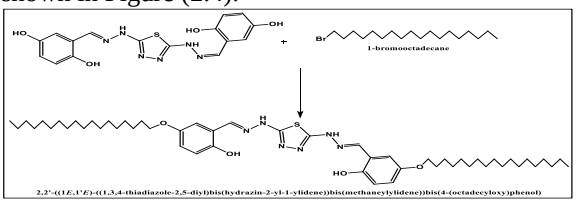

Figure 2.4: synthesis of Compound [BITT]

2.2.3 Synthesis of $Al_2O_3.B_2O_3$–[BITT] nanocomposite

$Al_2O_3.B_2O_3$–[BITT] was prepared according to N. Mir, et al., [33], modified method. First, (0.01 mole) of both compounds, $Al_2O_3.B_2O_3$ and [BITT], were dissolved in deionized water (20 ml). The mixture was refluxed at 60°C for 12 hours. The products were obtained through filtering and washed numerous times with ethanol. Solid powder and yield: 88**%** . as shown in Figure (2-5).

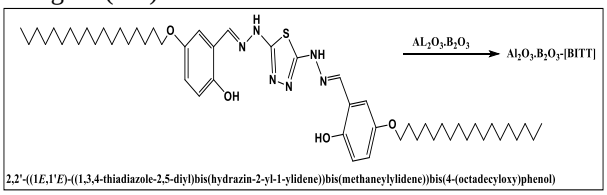

Figure 2.5: synthesis of nanocomposite $Al_2O_3.B_2O_3$–[[BITT]

2.4. structural and morphological properties: $Al_2O_3.B_2O_3$- BITT]:

The crystal structure of the aluminum borates nanoparticles and $Al_2O_3.$ B_2O_3- BITT] nanocomposite was investigated by X-ray diffraction (XRD, X'pert PW1730, Philips, US), Anode Material (Cu), K-Alpha1 [°A] (1.54060). Fourier transform infrared spectroscopy FT-IR was acquired at room temperature in the range of 400–3500 cm^{-1} using a spectrophotometer (Schimadzu 8601) via the KBr pellet method. A nuclear magnetic resonance spectrophotometer, model Ultrasheild 500 MHZ, was used to record ^{1}H-NMR spectra. (AFM), (SEM), and (TEM) were used for study particle prepared and morphology.

2.5. Corrosion Test

2.5.1. Sample preparation

In electrochemical corrosion test cell, the working electrode is carbon steel C1025. Each coupon should pass many preparation processes before the test. First step was the cutting of the metal coupon. Carbon steel C1025 was cutted as rectangular strips with dimension (length = 8 cm, width = 3 cm, and thickness = 0.1 cm). The dimensions are measured by a Vernier and the immersed part of coupon for corrosion test was marked to provide a total working electrode immersed area of (16.8 cm^2). These samples were polished with a belt grinding polishing machine and polished with papers of different grits (80,120,220, 320, 1200, and 2000) in sequence. After polishing, Carbon steel specimen was immersed in HCl solution (10 vol%) for (30) min, then washed with distilled water and deionized water and kept in ethanol absolute [34-36]. Polarization measurements were performed by automatically shifting the electrode voltage from +200 mV around OCP. To get corrosion data, the linear Tafel segments of anodic and cathodic curve areas were extrapolated to the corrosion potential. The potential scan started after the specimens were immersed in the test medium after (600 sec) [37- 40].

3: Results and discussion :

3.4.1 Atomic Force Microscopy (AFM) of $Al_2O_3.B_2O_3$

The surface morphology of $Al_2O_3.B_2O_3$ nanoparticles shows the 2D and 3D dimensional images of the Aluminum Borate nanoparticles before modification by the [BITT] compound, with a range diameter of between (47.86 -80nm). In addition to the determination of the particle size distribution, 2D and 3D views of AFM images for all applied layers were estimated. They revealed a smooth surface with grains nearly equal to the starting nanoparticles, as shown in Figure (3.1) .

3.1. X-ray diffraction

In order to characterize the nature of synthesized material, XRD pattern of the material was investigated. According to the XRD pattern shown in Figure3.1(a,b), the nanoparticles are identified as crystalline $Al_2O_3.B_2O_3$. It can be seen that the synthesized new nanocomposite consisted mainly of $Al_2O_3.B_2O_3$ and [BITT] . The X-ray diffraction pattern of nanoparticles $Al_2O_3.B_2O_3$ shown in Figure (3.2) indicated that the main phase of both samples was cuprospinel. The diffraction pattern of $Al_2O_3.B_2O_3$ nanoparticles showed sharp peaks at (25.61°), (32.78°), (35.18°), (37.74°), (43.52°), (52.67°), (57.82°), (66.76°), (68.54°) and (77.28°) corresponding to height of peaks (3004), (577), (5326), (2055), (6025),(2735), (2447) and (3107), respectively. The crystalline size of $Al_2O_3.B_2O_3$ nanoparticles was calculated by Scherer equation [41,42]. It was (30- 40) nm for $Al_2O_3.B_2O_3$. The peaks corresponding to $Al_2O_3.B_2O_3$ in $Al_2O_3.B_2O_3$ - [BITT] Figure (b) are weaker than those in pure $Al_2O_3.B_2O_3$ which shows that is covered with [BITT] composites

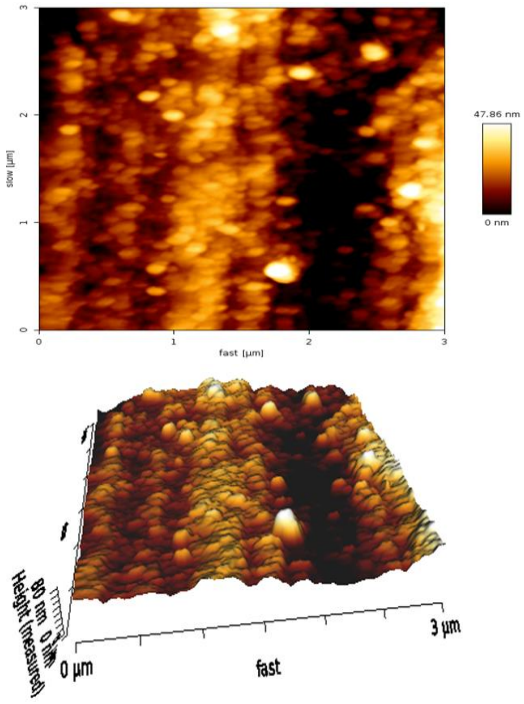

2D view 3D view

Figure(3.1): 2D and 3D views of AFM image of nanoparticles $Al_2O_3.B_2O_3$

.

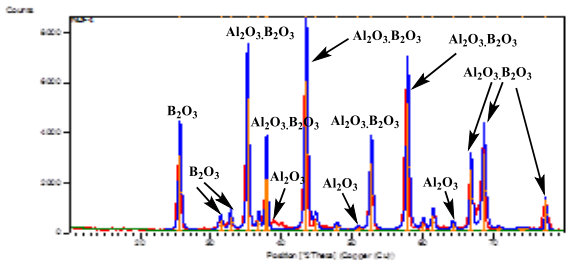

a=$Al_2O_3O.B_2O_3$

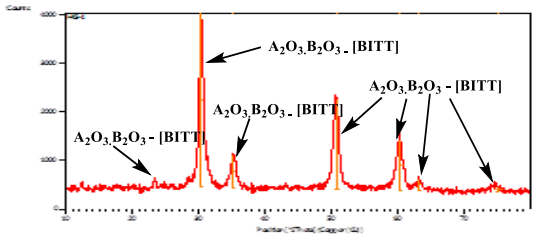

b= [BITT] –$Al_2O_3.B_2O_3$

Figure (3.2): XRD pattern of (a) Al_2O_3. B_2O_3 nanoparticles (b) Al_2O_3-[BITT] nanocomposite

2. FT-IR spectroscopy

FT-IR spectroscopy was utilized for characterization of the prepared nanocomposite. Figure3,3 (a, b) show the FT-IR spectra of $Al_2O_3.B_2O_3$ nanoparticles and [BITT]-$Al_2O_3.B_2O_3$, respectively. The primary detected peaks in (a) correspond to Al_2O_3-B_2O_3 nanoparticles. The (Al–O) vibration is given to the peaks near (593.88 cm^{-1} and 448.7 cm^{-1}). The (B–O) stretching vibration is responsible for the peak at (1109.97 cm^{-1}). The bands visible around (3442.68 cm^{-1}) are caused by the stretching and bending vibrations of the remaining H_2O and (Al-OH) groups. The overlapping stretching vibration of (B–O–B) bonds is assigned to the broad and strong peak around (1049.50 cm^{-1}) in both spectra [43-45]. Weak peaks in the range (1049.5–1700 cm^{-1}) indicates the attachment of $Al_2O_3.B_2O_3$ nanoparticles to the bond with [BITT] as shown in figure (b). The weak peak at 720.42 cm^{-1} in Figure (a) is referred to as C–S stretching vibration. The characteristic bands at (1636.76 and 1468.5 8 cm^{-1}) are attributable to stretching vibrations (C=N) and (C=C), respectively. The C–H stretching of the alkane chain is responsible for the apparent peak at (2849.43–2919.42 cm^{-1}). The O-H is assigned a single vibration at (3442.71 cm^{-1}) in the $Al_2O_3.B_2O_3$– [BITT] counterpart nanocomposite.

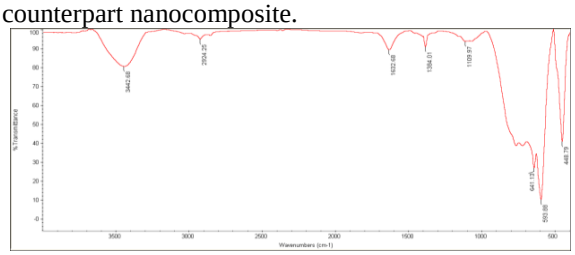

a= Al_2O_3. B_2O_3

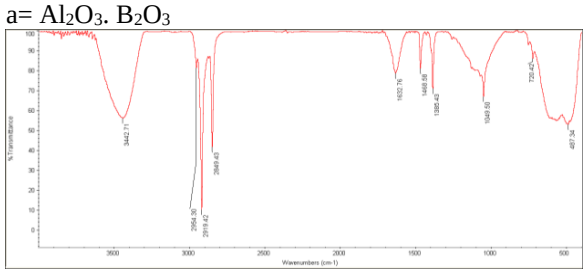

b=Al_2O_3. B_2O_3- [BITT]

Fig. 3.3: FT-IR spectra of (a) Al_2O_3. $B_2O_3$and (b) Al_2O_3. B_2O_3-[BITT]

3.3. ^{1}H NMR spectra of [BITT] Compound

1H NMR spectrum is shown in Figure (3·4), the spectrum is characterized by the appearance of the signals of The protons which are given rise as a signal in the following groups: ^{1}H-NMR data of (δ) in ppm : [(0.77 -0.98) ppm, triplet , - CH_3,6H], [(1.56 -1.70) ppm , Multiple,-CH_2 ,60 H , aliphatic chain], [(2.41 -2.52), hexet, -CH_2 ,4H] [(3.14-3.58) ppm , triplet,-CH_2 ,4H , linked to methoxy group],[(4.0-4-3.58) ppm ,Singlet, -CH,2H, schiff base protons],[(7.06-.7.27) ppm, Singlet NH,2H, the protons of amine group attached to the thiadiazole

ring] ,[(8.71) ppm, Singlet, (O-H), ,2H],[(7.06-8.59) ppm Multiple,C-H,6H, aromatic protons] .

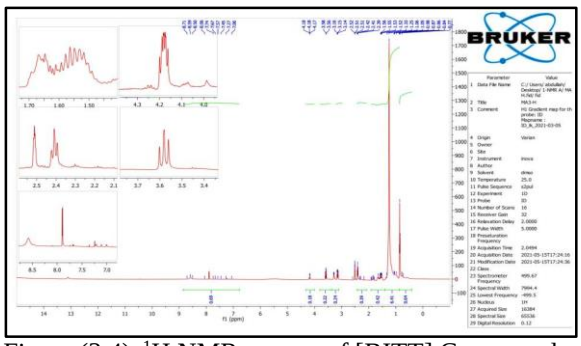

Figure (3.4): ^{1}H NMR spectra of [BITT] Compound

3.4. Field Emission Scanning Electron Microscopy Analysis (FESEM)

The FESEM image of the $Al_2O_3.B_2O_3$ nanocomposite and [BITT]-$Al_2O_3.B_2O_3$ is shown in Figure 3.5 (a-b). It indicates that $Al_2O_3.B_2O_3$ has particle sizes varying from (30 to 50 nm), which is in agreement with the crystallite size obtained from XRD data. The SEM image of the $Al_2O_3.B_2O_3$ showed a similar morphology to AFM images, but the clustering like shape observed led to the formation of highly agglomerated nanoparticles (cluster mass is made up of small particles) which are coherent together [46,47].

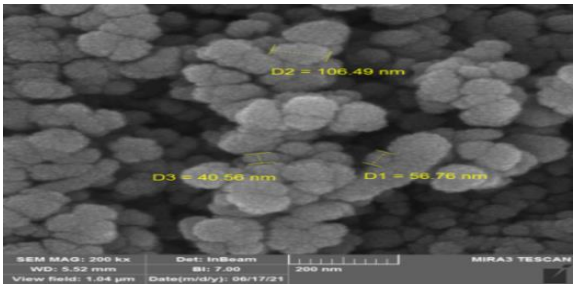

a: FESEM of $Al_2O_3.B_2O_3$

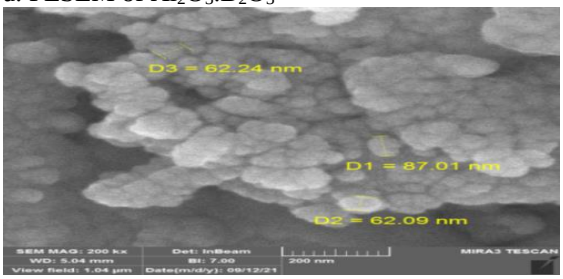

b: FESEM of $Al_2O_3.B_2O_3$–[BITT]

Figure (3.5) : FESEM of (a) $Al_2O_3.B_2O_3$ nanoparticles (b) $Al_2O_3.B_2O_3$-[BITT]

3.5. High-Resolution Transmission Electron Microscopy (TEM)

The morphology and average particle size of the prepared $Al_2O_3.B_2O_3$ and $Al_2O_3.B_2O_3$- [BITT] composite nanocomposites (TEM) were evaluated using transmission electron microscopy. Figures 3.6 (a,b) show TEM images of $Al_2O_3.B_2O_3$ and $Al_2O_3.B_2O_3$ [BITT] composites, respectively. The pictures revealed that the particles were in the nano size range and spherical in form, which is consistent with the XRD and FESEM results. The $Al_2O_3.B_2O_3$ nanoparticle layer on the [BITT] surface is visible in the TEM images of the $Al_2O_3.B_2O_3$-[[BITT] composite.

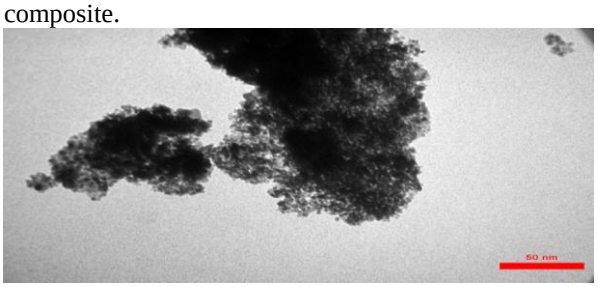

a: $Al_2O_3.B_2O_3$

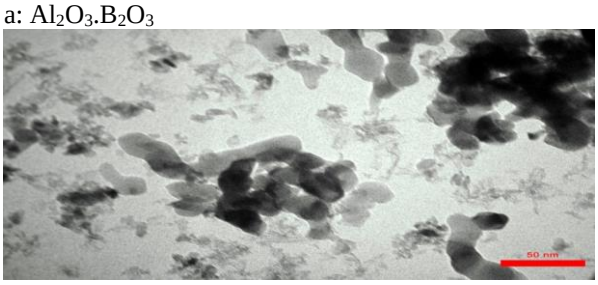

b: $Al_2O_3.B_2O_3$–[BITT]

Fig. 3.5: TEM of a: $Al_2O_3.B_2O_3$ and (b)$Al_2O_3.B_2O_3$–[BITT]

3.4. The Effect of $Al_2O_3.B_2O_3$ - [BITT] Inhibitors Concentration on the Corrosion Rate of Carbon Steel (C. 45) Specimens

The inhibitor nanocomposite $Al_2O_3.B_2O_3$-[BITT] was prepared in five different concentrations (100, 200, 300, 400, and 500 ppm).The inhibition efficiency was measured for each concentration at a constant time and temperature. Figure (3.7) demonstrates the anodic and cathodic polarization curves for the corrosion of carbon steel (C45) in 1M HCl. The extrapolation strategy for the polarization curves was connected and cathodic and anodic Tafel inclines (bc and ba) with consumption potential (Ecorr), corrosion current density (Icorr) and protective efficiency percentage (IE%) are recorded in Table (3.1). In addition, the inhibition efficiency of the prepared nanocomposite was calculated using the following equation:

$$IE\% = \left(1 - \frac{Icorr(inh)}{Icorr}\right) \times 100 \qquad \ldots\ldots\ldots(1)$$

Where Icorr(inh) is the inhibited corrosion current densities, Icorr(uninh) is the uninhibited current densities.

Table (3-1) shows the rate of corrosion in the presence of inhibitors is much less than in the absence of inhibitors. The corrosion resistance of the carbon

steel (C45) was reduced in the absence of $Al_2O_3.B_2O_3$-[BITT] nanocomposite inhibitor in the acidic medium HCl (1M) was equal to (36542 mpy), while in the presence of the prepared nano-corrosion inhibitor, the highest value of the carbon steel (C45) corrosion resistance was equal to (23.472 mpy).

From the table (3-1), it was found that by increasing the concentration of the $Al_2O_3.B_2O_3$-[BITT] inhibitor from 100 ppm to 500 ppm, the corrosion rate changed irregularly with an increasing concentration of the prepared inhibitory nanocomposite $Al_2O_3.B_2O_3$-[BITT], and this can be explained when all the active sites are saturated with the inhibitor, the growth of the inhibitor layer will gradually decrease with the increase in the concentration, as well as to the high compatibility between the chemical composition of the prepared inhibitory nanocomposite $Al_2O_3.B_2O_3$-[BITT] and the surface layer of the steel carbon (C.45) specimen surface. The highest value of the inhibition efficiency of the prepared nanocomposite was reached (%99.96) at concentration (100 ppm) .

Table 3-1: Electrochemical data acquired by Tafel plots for Specimens Carbon Steel (C. 45) in the absence and presence of $Al_2O_3.B_2O_3$ - [BITT] at 298 °K.

Comp.	Conc. ppm	C_R (MPY)	Rp (Ω*cm^2)	I_0 (Amp/ cm^{-2})	E_0 (V)	βa (mV)	βc (mV)	IE%	θ
HCl	1M	36542	0.22811	0.00789	-0.601	250	-684	0	0
$Al_2O_3.B_2O_3$-[BITT]	100	11.692	712.92	252×10^{-5}	-0.508	672	-107	99.96	0.9996
$Al_2O_3.B_2O_3$-[BITT]	200	23.472	355.12	507×10^{-5}	-0.480	765	-101	99.93	0.9993
$Al_2O_3.B_2O_3$-[BITT]	300	19.072	437.06	412×10^{-5}	-0.486	966	-105	99.94	0.9994
$Al_2O_3.B_2O_3$-[BITT]	400	19.057	437.39	412×10^{-5}	-0.480	707	-106	99.94	0.9994
$Al_2O_3.B_2O_3$-[BITT]	500	15.836	526.37	342×10^{-5}	-0.479	704	-106	99.95	0.9995

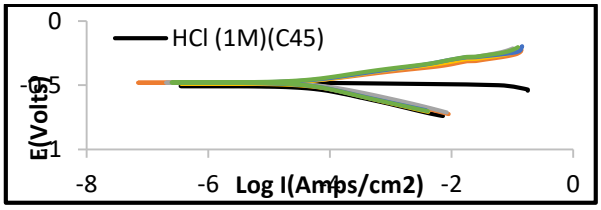

Figure 3.7: Tafel Plot for Specimen Carbon Steel (C. 45) absence and presence of $Al_2O_3.B_2O_3$ - [BITT] at 298 °K.

4.Conclusions

The characterization methods and surface morphology used in this work confirmed the composition of the prepared $Al_2O_3.B_2O_3$- [BITT] nanocomposite. The test results of prepared inhibitor show that, under the condition of different dosages of corrosion inhibitor, the inhibition efficiency is very high, and the increase or decrease in concentration did not affect the results of this efficiency, which indicates the high compatibility between the inhibited nanocomposite and the carbon steel (C45) surface. The results obtained can be summarized as:

1. The inhibitory action of the studied nanocomposite occurs as a result of the physically adsorption of the $Al_2O_3.B_2O_3$- [BITT] molecules on the metal surface.
2. From the results of the corrosion inhibition study of the prepared nanocomposite, it was found that the corrosion rate of the carbon alloy in the acidic medium reached very low levels.
3. The inhibition efficiency of the prepared nanocomposite is better than of using aluminum borate nanoparticles alone due to the increased adsorption of the nanocomposite due to the presence of functional groups.

Acknowledgements

The authors would like to express their gratitude to the referees and editors for their insightful comments. I also express my thanks and appreciation. Science college-Chemistry department/University of Thi-Qar/Iraq .

Refrences

[1] Y. Gogotsi,. Nanomaterials handbook. CRC press. vol. 46, no. 13. 2007.

[2 M. Nasrollahzadeh, M., Sajadi, M. S., Atarod, M., Sajjadi, M., & Isaabadi,
Z. An introduction to green nanotechnology. Academic Press, (2019).

[3] H. K. Farag, A. M. El-Shamy, E. M. Sherif, S. Z. El Abedin, Sonochemical Synthesis of Nanostructured ZnO/Ag Composites in an Ionic Liquid, Zeitschrift für Physikalische Chemie, 230 (12), 1733-1744. 2016

[4] Naeem A. Basher and Ali Abdulkhabeer Ali. "Hydrothermal Synthesis and Application of Nanocomposite as a Demulsifier in Crude Oil

Processing." Egyptian Journal of Chemistry 65.6: 1-2. 2022
[5] Ashraf K. Essa, A. M. El-Shamy, and Y. Reda. Fabrication of Commercial Nanoporous Alumina by Low Voltage Anodizing, Egypt. J. Chem. 61(1), 175-185. 2018.
[6] K. Sulabha. "Synthesis of nanomaterials-II (Chemical methods) .
" Nanotechnology: principles and practices. Springer, Cham, 77-109. 2015.
[7] K,Saebom. & C. Huh, "Use of nanoparticles for oil production applications,"
J. Pet. Sci. Eng., vol. 172, pp. 97–114, 2019.
[8] A. M. El-Shamy, M. F. Shehata, H. I. M. Metwally, A. Melegy, Corrosion and Corrosion Inhibition of Steel Pipelines in Montmorilonitic Soil Filling Material, Silicon, 10(6), 2809-2815. 2017.
[9] Amal M. Abdel-Karim, Ashraf M. El-Shamy, A Review on Green Corrosion Inhibitors for Protection of Archeological Metal Artifacts, Journal of Bio- and Tribo-Corrosion 8:35. 2022 .
[10] H. Hadi and T. J. Mohammed, "Improvement in demulsification of Iraqi crude oil with water removal demulsifiers in oil fields," IOP Conf. Ser. Mater. Sci. Eng., vol. 737, no. 1, 2020.
[11] C. Verma, E. E. Ebenso, and M. A. Quraishi, "Ionic liquids as green and
sustainable corrosion inhibitors for metals and alloys: An overview," J. Mol.
Liq., vol. 233, no. 2016, pp. 403–414, 2017.

[12] D. Abdeen, M. El Hachach, M. Koc, and M. A. Atieh, "A review on the
corrosion behaviour of nanocoatings on metallic substrates," Materials (Basel).,
vol. 12, no. 2, 2019.
[13] P. Rajeev, A. O. Surendranathan, and C. S. N. Murthy, "Corrosion mitigation of the oil well steels using organic inhibitors-A review," J. Mater. Environ. Sci., vol. 3, no. 5, pp. 856–869, 2012.
[14] A. Khudair, "The theoretical analysis of galanic corrsion (Zn , Fe and Cu) under activation control," 2009.
[15] H. Cen, Z. Chen, and X. Guo, "N, S co-doped carbon dots as effective corrosion inhibitor for carbon steel in CO_2 -saturated 3.5% NaCl solution," J. Taiwan Inst. Chem. Eng., vol. 99, pp. 224–238, 2019.
[16] L. Popoola, A. S. Grema, G. K. Latinwo, B. Gutti, and A. S. Balogun, "Corrosion problems during oil and gas production and its mitigation," Int. J. Ind. Chem., vol. 4, no. 35, pp. 1–15, 2013.
[17] M. Finšgar and J. Jackson, "Application of corrosion inhibitors for steels in acidic media for the oil and gas industry: A review," Corros. Sci., vol. 86, pp. 17–41, 2014.
[18] Y. Reda, H. M. Yehia, A. M. El-Shamy, Microstructural and mechanical properties of Al-Zn alloy 7075 during RRA and triple aging, Egyptian Journal of Petroleum ,31 , 9–13 . 2022.
[19] A. Samimiã and S. Zarinabadi, "An Analysis of Polyethylene Coating Corrosion in Oil and Gas Pipelines Amir," J. Am. Sci., vol. 7, no. 1, pp. 1032–1036, 2011.
[20] A. M. El-Shamy, M. F. Shehata, H. I. M. Metwally, A. Melegy, Corrosion and Corrosion Inhibition of Steel Pipelines in Montmorilonitic Soil Filling Material, Silicon, 10(6), 2809-2815. (2017).
[21]A. M. El-Shamy, M. F. Shehata, Samir T. Gaballah, Eman A. Elhefny, (Synthesis and Evaluation of Ethyl (4-(N-(thiazol-2-yl) Sulfamoyl) Phenyl) Carbamate as a Corrosion Inhibitor for Mild Steel in 0.1M HCl, Journal of Advances in Chemistry. 11(2), 3441-3451. 2014).
[22] T. Perez, "Corrosion in the oil and gas industry: An increasing challenge for materials," Jom, vol. 65, no. 8, pp. 1033–1042, 2013.
[23] Y. Reda, A. M. El-Shamy, Ashraf K. Eessaa, Effect of hydrogen embrittlement on the microstructures of electroplated steel alloy 4130, Ain Shams Engineering Journal 9(4), 2973-2982. (2018).
[24] K. M. Zohdy, R. M. El-Sherif, A. M. El-Shamy, Corrosion and Passivation Behaviors of Tin in Aqueous Solutions of Different pH, Journal of Bio- and Tribo-Corrosion 7(2), 1-7. (2021).
[25] V. Saji and R. Cook, Corrosion protection and control using nanomaterials, vol. 148. USA Philadelphia: Woodhead Publishing Limited, 2012.
[26] H .Hameed. Synthesis, Characterization of Some Nano Compound graphene oxide derivatives And Studying of their ability Corrosion Inhibitors for carbon Steel in Acidic media. Chemistry Department, College of Science, Univeristy of Basrah, Iraq , phD Thesis, 2018 .
[27] T. Quadri, L. O. Olasunkanmi, O. E. Fayemi, M. M. Solomon, and E. E. Ebenso, "Zinc Oxide Nanocomposites of Selected Polymers: Synthesis, Characterization, and Corrosion Inhibition Studies on Mild Steel in HCl Solution," ACS Omega, vol. 2, no. 11, pp. 8421–8437, 2017.
[28] K. Vinothkumar and M. G. Sethuraman, "Corrosion inhibition ability of electropolymerised composite film of 2-amino-5-mercapto-1,3,4-thiadiazole/TiO2 deposited over the copper electrode in neutral medium," Mater. Today Commun., vol. 14, pp. 27–39, 2018.

[29] V. Tan, L. The Vinh, L. Tu Quynh, H. Thu Suong, and H. Dang Chinh, "A novel synthesis of nanoflower-like zinc borate from zinc oxide at room temperature," Mater. Res. Express, vol. 7, no. 1, pp. 1–9, 2020.
[30] N.A. Basher, I. A. Flifel, and A. A. Mashaf, "Synthesis, Characterization and antibacterial Study of some Complexes Derivatives from1,3,4-

Thiadiazole Schiff base," IOP Conf. Ser. Mater. Sci. Eng., vol. 928, no. 5, 2020.
[31] N.A. Basher, "Study of New Derivatives of 1,3,4-Thiadiazole and Its Complexes with chromium ion (Cr^{+3})," IOP Conf. Ser. Mater. Sci. Eng., vol. 928, no. 5, 2020.
[32] A. Ayyash, H. J. Jaffer, and J. H. Tomma, "Synthesis and characterization of some novel 4-thiazolidinones and isoxazolines derived from thiosemicarbazones," Am. J. Org. Chem., vol. 4, no. 2, pp. 52–62, 2014.
[33] N. Mir, S. Jalilian, P. Karimi, M. Nejati-Yazdinejad, and S. Khammarnia, "1,3,4-Thiadiazol derivative functionalized-Fe3O4@SiO2 nanocomposites as a fluorescent probe for detection of Hg2+ in water samples," RSC Adv., vol. 8, no. 39, pp. 21745–21753, 2018.
[34] M. Ajmal, A. S. Mideen, and M. A. Quraishi, "2-hydrazino-6-methyl-benzothiazole as an effective inhibitor for the corrosion of mild steel in acidic solutions," Corros. Sci., vol. 36, no. 1, pp. 79–84, 1994.
[35] N. Muhsin, Hayder. K., Noor, D., Aljamali, M., & Nawfel, M. Preparation of chemical inhibitors to treat the corrosion and erosion of machines. International Journal of Engineering, Applied and Management Sciences Paradigms, 54(3), 89-93G, 2019.
[36] R. Agrawal and T. K. G. Namboodhiri, "The inhibition of sulphuric acid corrosion of 410 stainless steel by thioureas," Corros. Sci., vol. 30, no. 1, pp. 37–52, 1990.
[26] M. Kadhum, "Synthesis , Identification and Study of Some New Schiff Bases as Inhibitors for Brass Corrosion and Bacterial Growth," J. Basrah Res., vol. 37, no. 2, 2011.
[37] L. Larabi, O. Benali, S. M. Mekelleche, and Y. Harek, "2-Mercapto-1-methylimidazole as corrosion inhibitor for copper in hydrochloric acid," Appl. Surf. Sci., vol. 253, no. 3, pp. 1371–1378, 2006.
[38] F. Hong-bo, W. Hui-long, G. Xing-peng, and Z. Jia-shen, "Corrosion inhibition mechanism of carbon steel by sodium N, N-diethyl dithiocarbamate in hydrochloric acid solution," Anti-Corrosion Methods Mater., vol. 49, no. 4, pp. 270–276, 2002.
[39] S. Rajendran, S. M. Reenkala, N. Anthony, and R. Ramaraj, "Synergistic corrosion inhibition by the sodium dodecylsulphate–Zn2+ system," Corros. Sci., vol. 44, no. 10, pp. 2243–2252, 2002.
[40] V. Saji and S. A. Umoren, Corrosion Inhibitors in the Oil and Gas Industry. Weinheim, Germany: Wiley-VCH Verlag GmbH, 2020.
[41] P. Y. Hou, X. F. Zhang, and R. M. Cannon, "Impurity distribution in
Al_2O_3 formed on an FeCrAl alloy," Scripta Materialia, vol. 50, no. 1,
pp. 45–49, 2004.
[42] B. D. Cullity, Elements of XRD, Addison-Wesley, Reading,Mass, USA,
2nd edition, 1978.
[43] L. Shen, C. Hu, Y. Sakka, and Q. Huang, "Study of phase transformation
behaviour of Al_2O_3 through precipitation method," Journal of Physics D:
Applied Physics, vol. 45, no. 21, 2012.
[44] C.H. Shek, J. K. L. Lai, T. S. Gu, andG.M. Lin, "Transformation evolution
and infrared absorption spectra of amorphous andcrystalline nano- Al_2O_3
powders," Nanostructured Materials, vol. 8, no. 5, pp. 605–610, 1997.
[45] Saffari, H. R. M., et al. "Tribological properties of water-based drilling fluids with borate nanoparticles as lubricant additives." Journal of Petroleum Science and Engineering 171: 253-259. 2018.
[46] D. Naumenko, W. J. Quadakkers, A. Galerie, Y. Wouters, and S. Jourdain,
"Parameters affecting transient oxide formation on FeCrAl based foil and
fibre materials," Materials at High Temperatures, vol. 20, no. 3, pp. 287–
293, 2003.
[47] W. J. Quadakkers, J. Nicholls, D. Naumenko, J. Wilber, and L Singheiser,Materials Aspects in Automotive Catalytic Converters MACC, H. Bode, Ed.,Wiley-VCH, Munchen, Germany, 2001.

.